Volume 3 | Number 18 | 14 May 2015 | Pages 9323–10138

Journal of Materials Chemistry A

Materials for energy and sustainability

www.rsc.org/MaterialsA

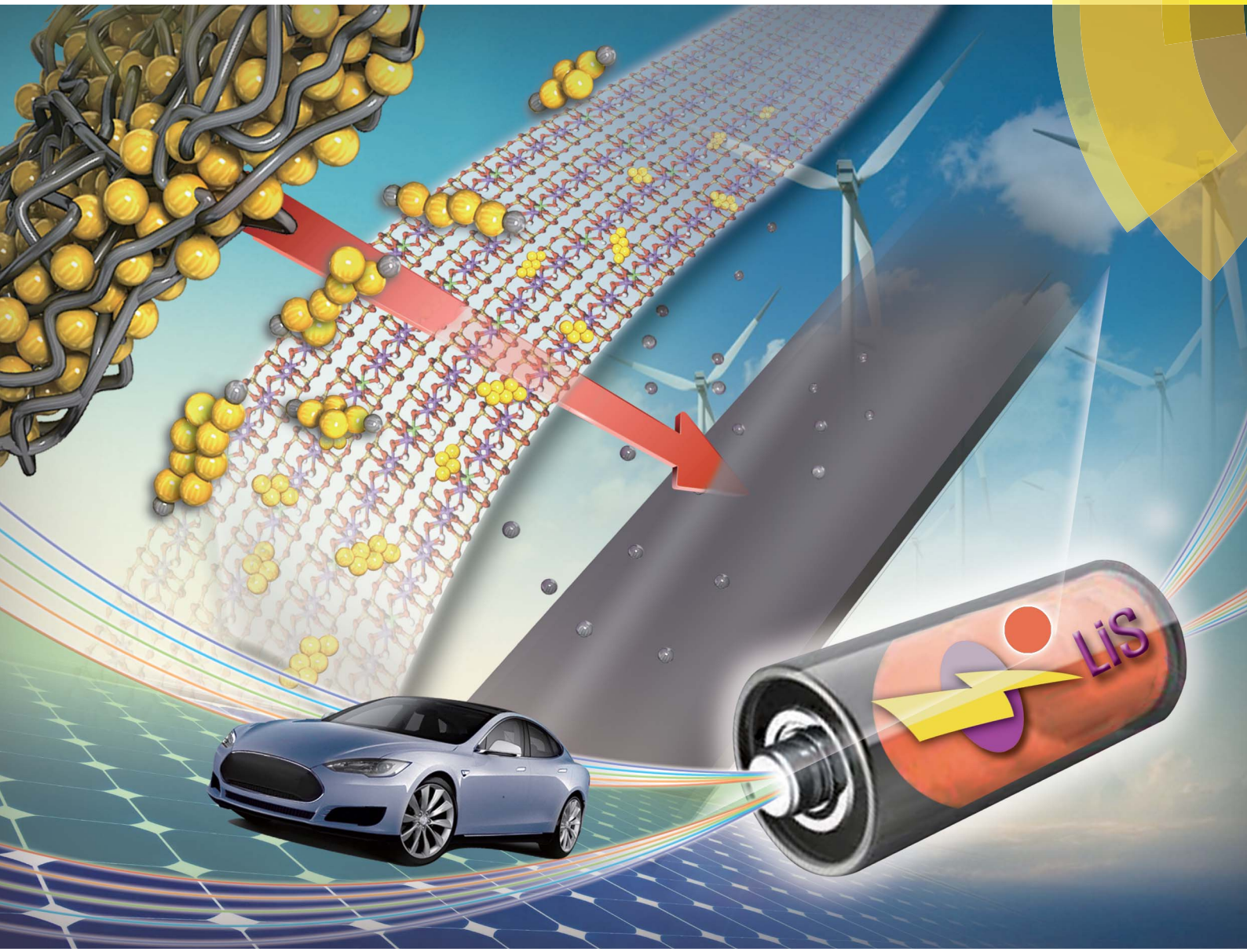

ISSN 2050-7488

ROYAL SOCIETY OF CHEMISTRY

PAPER

Wook Ahn, Sun-Hwa Yeon *et al.*

Interaction mechanism between a functionalized protective layer and dissolved polysulfide for extended cycle life of lithium sulfur batteries

Journal of Materials Chemistry A

PAPER

View Article Online
View Journal | View Issue

Cite this: J. Mater. Chem. A, 2015, 3, 9461

Interaction mechanism between a functionalized protective layer and dissolved polysulfide for extended cycle life of lithium sulfur batteries

Wook Ahn,*[a] Sung Nam Lim,[b] Dong Un Lee,[a] Kwang-Bum Kim,[c] Zhongwei Chen[a] and Sun-Hwa Yeon*[d]

Received 20th February 2015
Accepted 11th March 2015

DOI: 10.1039/c5ta01378j

www.rsc.org/MaterialsA

To improve the cycle life of Li–S rechargeable batteries, chemically dispersed nanocarbon materials are usually employed as adsorbents and conductive matrices for cathodic nano-sized sulfur materials. Herein, a new assembly for Li–S cells is developed by introducing a montmorillonite (MMT) ceramic protective film to form an ion selective separator. The effect of the MMT-coated separator and the reaction mechanism between MMT and polysulfides are characterized *via* Raman and zeta potential analyses. The utilization of the MMT coated separator enables the minimization of the shuttle effect by preventing the diffusion of polysulfide. The best discharge capacity and cycle life are obtained with the MMT coated separator in a sulfur–MWCNT composite cathode, resulting in a discharge capacity of 1382 mA h g^{-1} at a current density of 100 mA g^{-1} and 924 mA h g^{-1} after 200 cycles. The Li–S cell using the nano-sized sulfur–MWCNT composite and the MMT-coated separator shows significantly excellent electrochemical performance.

Introduction

In recent years, there has been a great demand for lithium rechargeable batteries with high theoretical power outputs and energy densities due to the development of high performance electric vehicles (EVs) and portable electric devices.[1–3] At present, among the commercially available rechargeable lithium-based batteries, lithium-ion batteries (LIBs) normally generate specific energies in the range of 100 to 200 W h kg^{-1}.[4] Even though the cathode materials used in LIBs produce relatively low specific capacities, they are still in demand for high power and high energy density applications. To meet the requirements of both high power and high energy applications, a breakthrough in lithium based rechargeable batteries is much needed. In this regard, lithium–sulfur batteries have gained particular interest due to their high theoretical capacity (1675 mA h g^{-1}) and energy density (2600 W h kg^{-1}). Additionally, lithium–sulfur batteries properly operate even at very low temperatures, again ideal for EV and portable electronic applications.[5] Furthermore, sulfur is a relatively much cheaper material than intercalation materials, which makes lithium–sulfur batteries extremely cost effective. However, lithium–sulfur batteries still suffer from capacity diminution with advancing cycles and a low electronic conductivity of sulfur itself.[6,7] The capacity fading with advancing cycles results from the formation of highly soluble lithium polysulfide intermediates in non-aqueous electrolytes during the cycling process. For this battery system, the most significant solution is preventing the diffusion of lithium polysulfides.[8–10] Almost all published studies on lithium–sulfur batteries have focused on solving these problems in respect of the electrode material, membrane, and electrolyte. In order to improve the capacity and prevent the dissolution of lithium polysulfides, carbon-based sulfur composites obtained through various fabrication routes have previously been utilized as cathode materials, such as, the sulfur-impregnated carbon nanotubes or sulfur nanofiller composites constrained in a porous carbon framework.[6,7,11–14] Also, in our previous work, a chemically dispersed sulfur–MWCNT composite as a cathode material was synthesized *via* a simple direct precipitation route.[15,16] In another respect, various membrane treatments using some coating processes on a separator have been utilized to enhance the cyclability. The use of a coating prepared by phase inversion using montmorillonite (MMT) has been well known as a good method for improving the physical and electrochemical stability of LIBs, and its high thermal and mechanical properties help to eliminate short-circuit issues caused by dendritic growth of lithium on the electrode surface.[17–21] In general, well-dispersed clay particles in a polymeric matrix can improve

[a]Department of Chemical Engineering, University of Waterloo, 200 University Ave W., Waterloo, ON, N2L3G1, Canada. E-mail: wahn@uwaterloo.ca; Fax: +1-519-888-4347; Tel: +1-519-888-4567 ext. 31614

[b]Department of Chemical & Biomolecular Engineering, Korea Advanced Institute of Science and Technology, 291 Daehak-ro, Yuseong-gu, Daejeon 305-701, Korea

[c]Department of Materials Science & Engineering, Yonsei University, 50 Yonsei-ro, Seodaemun-Gu, Seoul, 120-749, Korea

[d]Korea Institute of Energy Research, 152 Gajeong-ro, Yuseong-Gu, Daejeon, 305-343, Korea. E-mail: ys93@kier.re.kr; Fax: +82-42-860-3133; Tel: +82-42-860-3763

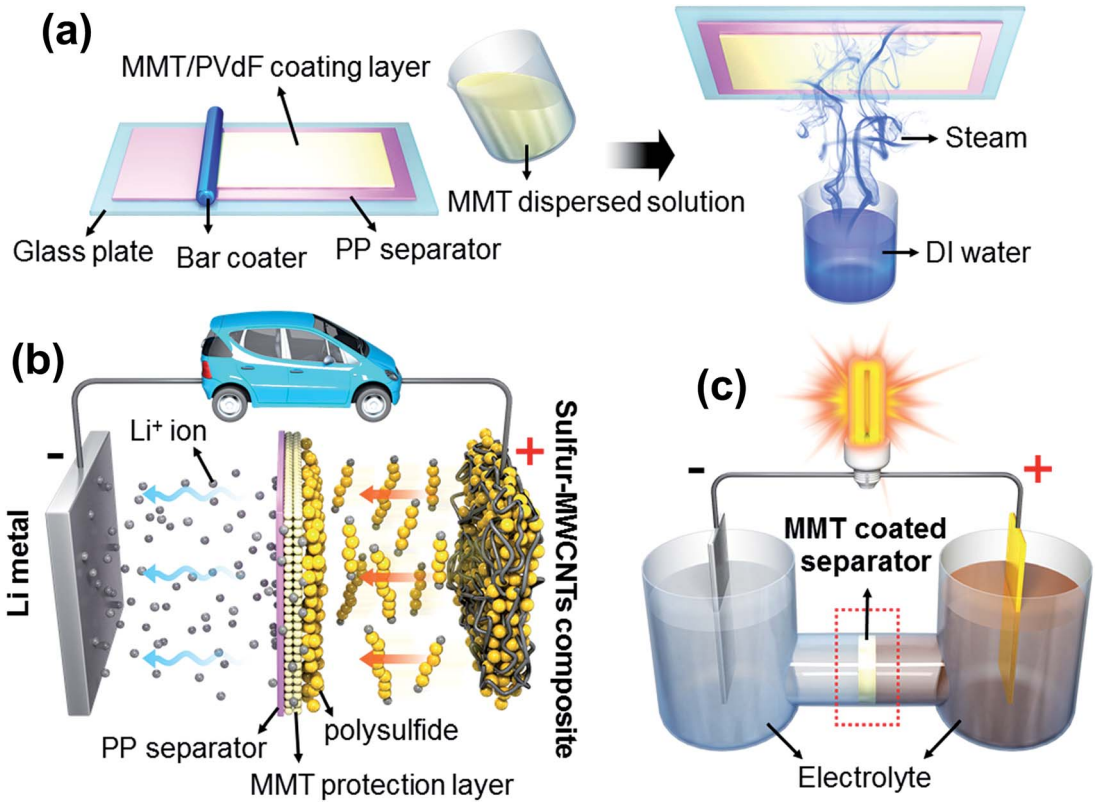

Fig. 1 Schematic configuration of the preparation procedure of the MMT coated separator (a), theoretical mechanism of the Li–S cell using the MMT coated separator (b) and the electrochemical cell for Raman analysis (c).

the thermal and mechanical properties of films,[22] and hydrophilic MMT can provide enhanced wettability in liquid electrolytes.[23] However, to the best of our knowledge, the MMT coating has never been implemented in a Li–S battery system as a protective layer for preventing the diffusion of lithium polysulfides. In this work, we have demonstrated excellent electrochemical properties, for the first time, by using a MMT coated protective PP layer as an effective separator for preventing the dissolution of lithium polysulfides in a Li–S battery system. Simultaneously, the sulfur–MWCNT composite has been used as the cathode[15,16] and investigated by Raman spectroscopy to examine the behavior of lithium polysulfide within the lithium sulfur cell during the charge–discharge processes. The manufacturing process of the MMT coated separator and electrochemical cell for Raman study is presented in Fig. 1.

Experimental section

Preparation of the sulfur–MWCNT composite and MMT coated separator

The synthesis of the sulfur–MWCNT composite and the manufacturing procedure of the MMT coated separator are presented in Fig. 1. The detailed preparation of the sulfur–MWCNT composite using the direct precipitation method has been described previously in the "Direct precipitation method".[16] In order to synthesize the sulfur–MWCNT composite, MWCNTs were dispersed in a 0.1 mol $Na_2S_2O_3$ solution with vigorous mixing. Then the solution was sonicated for 2 h, after which a 0.1 mol H_2SO_4 solution was added dropwise into this solution at a rate of 10 mL min^{-1}. In order to adjust the amount of precipitated sulfur (3.88 g) in the composite, the amount of MWCNTs added to the solution was 0.97 g producing a weight ratio (sulfur : MWCNTs) of approximately 80 : 20 in the final composite.

The preparation of the MMT (montmorillonite: Sigma-Aldrich, K 10) coated separator was conducted using a simple casting process and phase inversion of the MMT clay using distilled water. The procedure is as follows: 1.5 g PVdF-HFP co-polymer (Kynar 2801) was used as a binder in a mixed solution of 7 g *N*-methyl propylene and 5 g of acetone, using a paste mixer. Then 1.5 g of MMT powder was gradually added into the solution, and stirred using a planetary mixer for 4 hours at room temperature. After vigorous mixing, the mixture was coated on a separator (Celgard 3501) to 25 μm thickness using a bar-coater. The coated separator was then dried at room temperature for 1 hour. In order to conduct the phase inversion of the MMT clay, it was exposed to steam from boiling distilled water for 10 minutes. After the phase inversion, the MMT-coated separator was dried in an oven at 60 °C for 24 hours under vacuum. The final loading of the MMT-copolymer protective layer on the PP separator was 1.65 mg cm^{-2} (MMT: 0.825 mg cm^{-2}, PVdF-*co*-HFP: 0.825 mg cm^{-2}).

Characterization: physical and electrochemical properties

To confirm the amount of sulfur content in the sulfur–MWCNT composite, thermogravimetric analysis (TGA/SDTA851^e-METTLER) was performed across a temperature range of 25–600 °C at a 5 °C min^{-1} heating rate in air. For the structural analysis, X-ray diffraction of the phases was carried out using a HPC-2500 XRD (Gogaku) with Cu Kα radiation (λ = 1.5405 Å) in the 2θ range of 10–80° with 0.02° intervals, at a 2° min^{-1} scanning rate. The morphology of the synthesized sulfur–MWCNT composite and the MMT-coated separator was analyzed using a scanning electron microscope (SEM; S4700, Hitachi). In order to quantify the lithium polysulfide in the electrolyte and on the side of the cathode, Raman spectrometry (DXR Raman Microscope, Thermo Fisher Scientific) with a frequency diode laser at 532 nm was used. The electrochemical cell for Raman analysis was evaluated and the schematic diagram is presented in Fig. 1. After manufacturing an electrolyte test cell, the charge–discharge across 5 cycles was examined. In order to verify the driving force between MMT and polysulfide, the zeta potential (ELS-8000, Otasuka Electronics Co.) of MMT was measured.

For electrochemical testing, the cathode electrodes were prepared by mixing 20 wt% PVdF-HFP co-polymer (Kynar 2801) as a binder and 80 wt% of the sulfur–MWCNT composite in *N*-methyl-2-pyrrolidone (NMP), then this slurry was mixed using a planetary mixer with a zirconia ball for 3 h to achieve a uniform mix. This slurry was then coated on Al foil (20 μm) to 60 μm thickness using a doctor blade to form the cathode. The electrode was pressed using a twin roller and dried at 70 °C under a vacuum. The final thickness of the cathode material on the Al foil was 50 μm, and the sulfur loading was 0.7 mg cm^{-2}. CR2032 coin-type cells were assembled using 1.0 M $LiCF_3SO_3$ and 0.2 M $LiNO_3$ in a mixture of tetra(ethylene glycol)dimethyl ether (TEGDME)–1,3-dioxolane (DOL) (50 : 50 vol%) as an electrolyte. Lithium foil was used as the counter electrode. The electrode had a size of 14Ø and 80 μL of the electrolyte was injected. Both an uncoated and a MMT-coated separator were used as separators in the test cells. In order to verify the influence of the MMT-coated separator, the side coated with MMT was placed facing the cathode. The entire procedure for the coin cell assembly was performed in an argon (Ar) filled glove box. Fabricated coin cells were aged for 2 h at room temperature in an oven. Then the charge and discharge cycles were carried out (MACCOR 4000 SERIES) at a current density of 100 mA g^{-1} (based on sulfur) within a voltage range between 1.6 and 2.8 V at room temperature.

Results and discussion

Fig. 2(a) presents the XRD pattern of the sulfur–MWCNT composite, and all the measured peak positions correspond to the sulfur octatomic molecules with S_8 which is highly polymorphic and forms an orthorhombic phase (α-S_8) with the space group *Fddd* (JCPDS 83-2283). Also, there are no peaks related to impurities except for the slightly broadened XRD peak around *ca.* 26° due to the well-dispersed MWCNTs, indicative of homogeneity of the composite obtained by the direct precipitation method. Fig. 2(b) shows the TGA-DTA results of the mixed precursor powder from 25 °C to 600 °C under a nitrogen atmosphere. There is only one weight loss stage apparent in the TGA curve. The abrupt weight loss in the 25 °C–350 °C temperature range reflects the sulfur decomposition and the weight loss is approximately 75 wt%, in accordance with our previous work.[16]

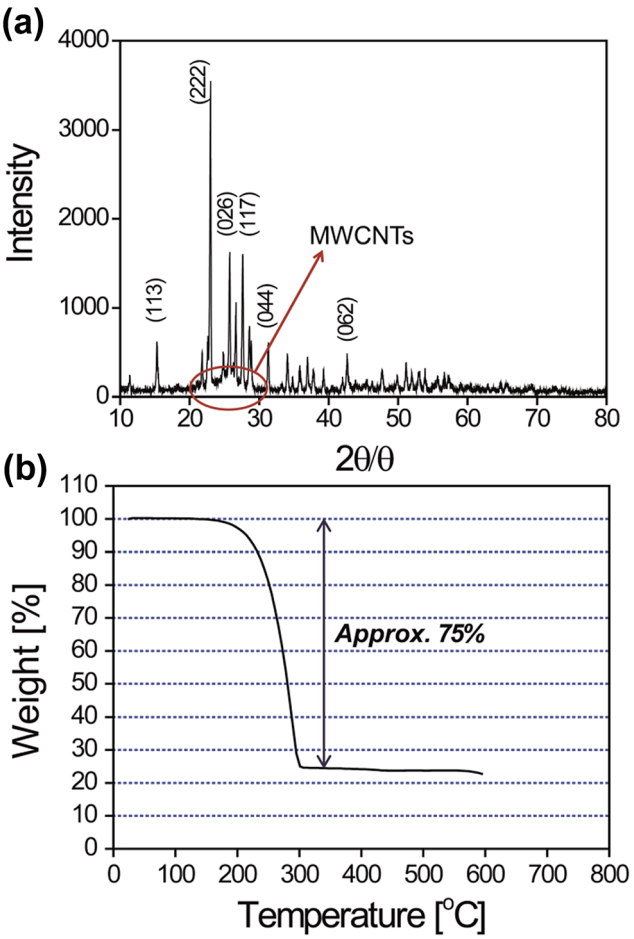

Fig. 2 XRD pattern (a) and TGA results (b) of the sulfur–MWCNT composite.

Fig. 3(a) shows the SEM image of synthesized sulfur–MWCNTs. It is apparent in Fig. 3(a) that the MWCNTs and the precipitated sulfur are intertwined, implying that the precipitated sulfur is dispersed uniformly. The MWCNT uniformity in the composite is shown by EDS maps presented in Fig. 3(b) and (c), with the bright spots indicating the presence of carbon and sulfur elements, respectively. The EDS mapping results demonstrate that sulfur is well distributed throughout the entire surface of MWCNTs through the direct precipitation method.

Fig. 4(a) and (d) show the SEM images of the as-received PP separator and MMT-coated separator before the electrochemical test, respectively. From Fig. 4(d), it is clear that the MMT particles are well dispersed on the separator surface with excellent uniformity. The used cathode-side and anode-side of the as-received separator after electrochemical tests are

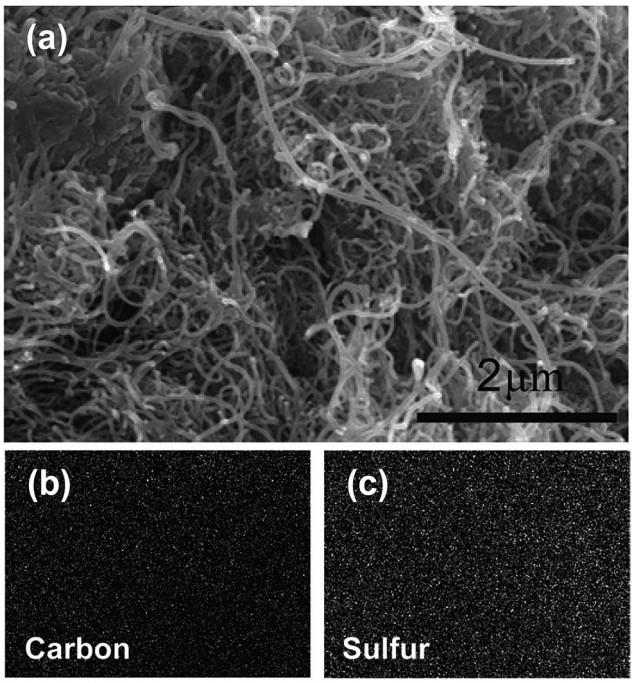

Fig. 3 SEM image (a) and EDS mapping results ((b) carbon, (c) sulfur) obtained from the sulfur–MWCNT composite.

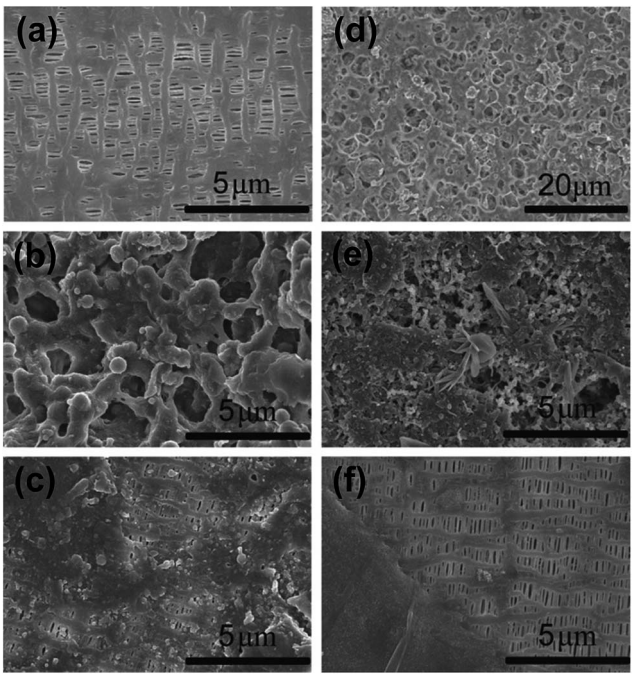

Fig. 4 SEM images of the as-received separator: before the electrochemical test (a), front side (b) and back side (c) after the test; MMT-coated separator: before the electrochemical test (d), front side (e) and back side (f) after the cell test.

presented in Fig. 4(b) and (c) and those of the MMT coated separator are shown in Fig. 4(e) and (f), respectively. It could be verified that the dissolved polysulfide is covered on the surface of the cathode-side of the two separators (Fig. 4(b) and (e)).

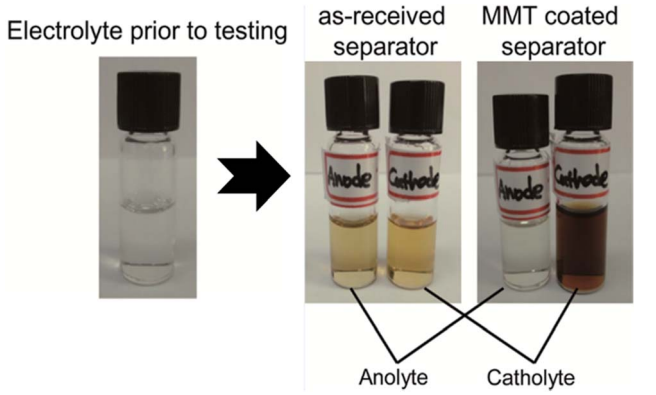

Fig. 5 The colour change comparison of the catholyte and the anolyte employing the as-received separator and MMT-coated separator.

However very interestingly, the anode-side (Fig. 4(c)) of the as-received separator is also covered with the diffused polysulfide, whereas that of the MMT-coated separator (Fig. 4(f)) is still pristine and the pores for lithium ion transportation are sustained. Therefore, SEM observation strongly suggests that a simple MMT coating is extremely effective in preventing the diffusion of polysulfide through the separator. When sulfur molecules react with lithium ions, they become soluble lithium polysulfides (when using organic electrolytes) which cause the problem of rapid capacity decay in lithium sulfur batteries.[24–26] When this occurs, the color of the organic electrolyte changes from white to brown or dark brown. It is known that the dissolved lithium polysulfides in the electrolyte lead to the shuttle mechanism.[6–8] Once the lithium polysulfide is dissolved, it can easily diffuse to the anode side, suppressing the reduction of lithium ions to lithium metal. This irregular reaction leads to an infinite charge and decreases the capacity.[26,27] The MMT coated layer on the separator prevents the diffusion of polysulfide anions through the separator, restricting the shuttle mechanism. In order to evaluate the protecting function, both the MMT-coated and the as-received separators (Celgard 3501) are compared after electrochemical testing. Fig. 5 shows the color comparison for the catholyte and the anolyte after using the two separators. The tested cell for the separation of the electrolyte after testing has been prepared as shown in Fig. 1(c). In the case of the as-received separator, the catholyte and anolyte on both sides of the electrode changed to a thin dark brown color. However, while the anolyte of the MMT-coated separator remained unchanged, the catholyte of that was changed to heavy dark brown. This is clear visual evidence that the MMT-coating layer prevents lithium polysulfide diffusion to the anode.

Fig. 6(a)–(c) show the optical microscopy images of the MMT coated separator prior to testing (a) and the cathode side (b) and anode side (c) after testing. The surface of the cathode side (b) after cycling shows the accumulated lithium polysulfide. Also, it appears that the surface colour of the anode side has changed to silver, resulting from the lithium sulfides accumulated on the surface and/or in the separator pores. The optical microscopy images of the as-received separator before (d) and after testing

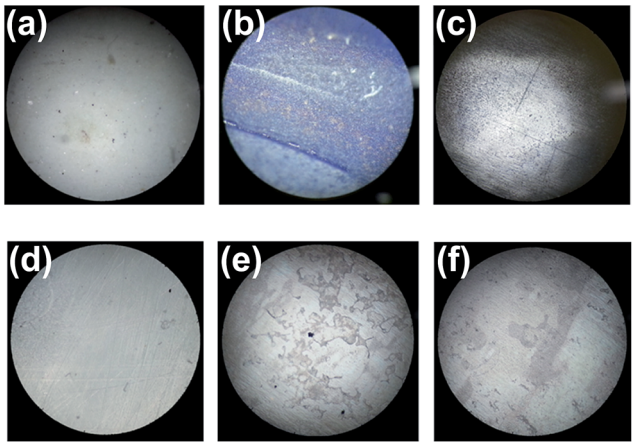

Fig. 6 Optical images of the MMT coated separator ((a) prior to testing, (b) cathode side after testing, (c) anode side after testing); and the as-received separator ((d) prior to testing, (e) cathode side after testing, (f) anode side after testing).

(e) and (f) are presented in Fig. 6, respectively. The surfaces of both sides of the PP separator have changed to a partially stained color, indicating that the dissolved lithium polysulfide has diffused to the anode side. From these microscopy images and the color changes observed in Fig. 5, it is evident that the dissolved lithium polysulfide is accumulated only on the MMT-coated cathode side during the electrochemical reduction and oxidation cycles, preventing polysulfide diffusion to the anode side thereby suppressing the shuttle mechanism caused by lithium polysulfide formation.

To further investigate the effectiveness of the MMT coated separator, Raman spectroscopy has been utilized to study various battery components. Fig. 7(a) and (b) show comparative Raman analyses of the catholyte and the anolyte before and after testing of the electrochemical cell (Fig. 1(c)) containing the as-received separator (Fig. 7(a)) and MMT-coated separator (Fig. 7(b)), respectively. The electrolyte prior to testing shows pronounced peaks at 314, 348, 759, 942, 1043, 1231, 1477, 2765, 2891 and 2955 cm^{-1}. The intensity of these peaks decreased for both sides of the as-received separator after testing. After testing, broad peaks, representative of lithium polysulfide, appeared at approximately 2200 and 2800 cm^{-1}. The strong peaks at 2765, 2891 and 2955 cm^{-1} observed in the electrolyte before the testing disappeared after that. For the MMT-coated separator sample (in Fig. 7(b)), while the strong peaks at 2765, 2891 and 2955 cm^{-1} in the catholyte have also disappeared, the broad weak peaks of lithium polysulfide (2436 and 2552 cm^{-1}) are revealed. However, the electrolyte on the anode side of the MMT-coated separator after the cell test remains unchanged, further making the MMT coated layer suppress the lithium polysulfide diffusion to the anode side.

Fig. 8 presents the Raman spectra obtained from pure sulfur, the sulfur–MWCNT composite and Li_2S (theoretically the material left after full discharge). The pristine sulfur shows strong Raman modes of sulfur at 151, 217 and 471 cm^{-1}. The Raman spectra of the synthesized sulfur–MWCNT composite show the same Raman modes of sulfur as well as the G, D and

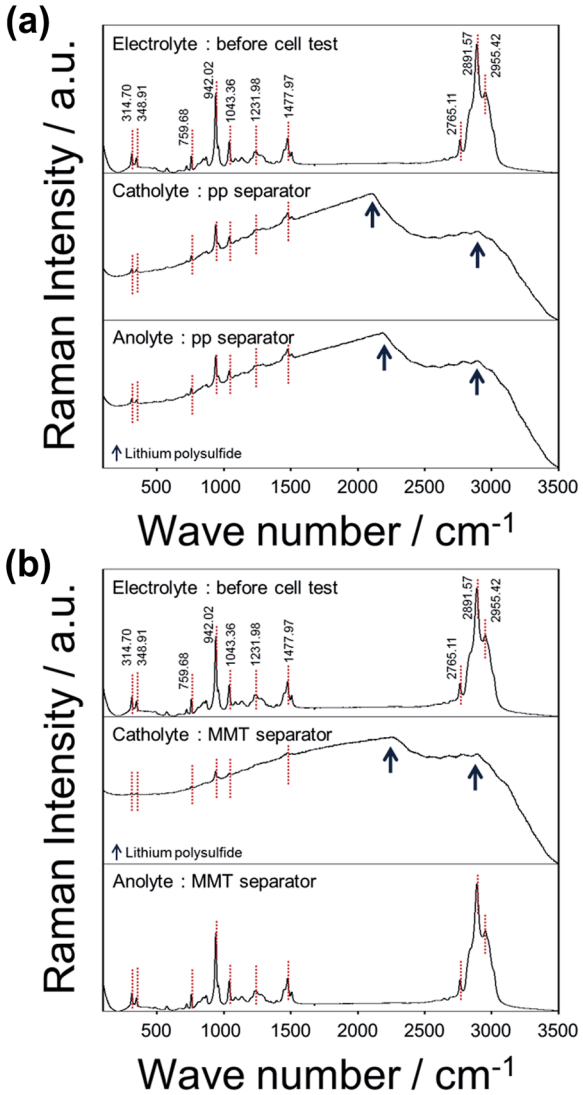

Fig. 7 Raman study results for the electrolyte using (a) the PP separator before the electrochemical test and after the test; (b) MMT-coated separator before the electrochemical test and after the test.

2D peaks of MWCNTs. The fully discharged electrode sample shows strong main peaks of 372 and 481 cm^{-1} and weak peaks at 2436 and 2552 cm^{-1}, which correspond to lithium sulfides (strong Raman mode) and lithium polysulfide (weak Raman mode) produced during the Li–S reaction, respectively.[28] To identify the interaction mechanism between MMT and polysulfide anions during the charge–discharge process, the zeta potential is measured using a reference solvent. The zeta potential results of MMT dispersed in deionized water (DI) and in 2-propanol gave respective values of −96.18 mV and −63.34 mV (Fig. 9), confirming the driving force between MMT and polysulfide anions, since polysulfide exists as an anion in the organic electrolyte and the MMT is also negatively charged. These intrinsic characteristics indicate that the repulsive forces between MMT and polysulfide anions interact with each other, leading to a stable performance. If MMT has a positive charge in the electrolyte, the dissolved polysulfide is adsorbed onto MMT.

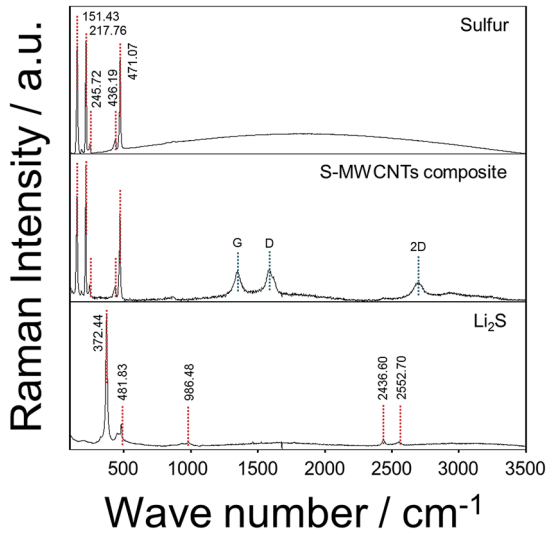

Fig. 8 Raman study results of materials (sulfur, sulfur–MWCNT composite and Li_2S).

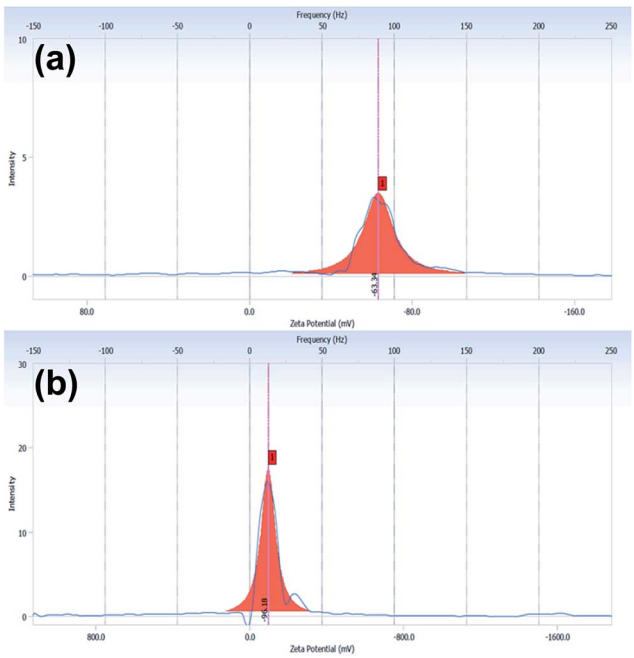

Fig. 9 Zeta potential results of the MMT powder ((a) dispersed in DI, (b) dispersed in 2-propanol).

Then, the concentration of polysulfide would become lower in the electrolyte, leading to the additional dissolution of the active material to adjust the intrinsic solubility of polysulfide in the organic electrolyte. Therefore, the dissolved polysulfide is blocked from diffusing through the separator due to the repulsive ionic forces, proving the reaction mechanism of the MMT-coated separator when used as a protective layer. Based on this result, it is assumed that the bond of highly ordered lithium polysulfide is broken by the repulsive interaction between the MMT anion and polysulfide anion during the charge process, leading to the reduction of metallic lithium on

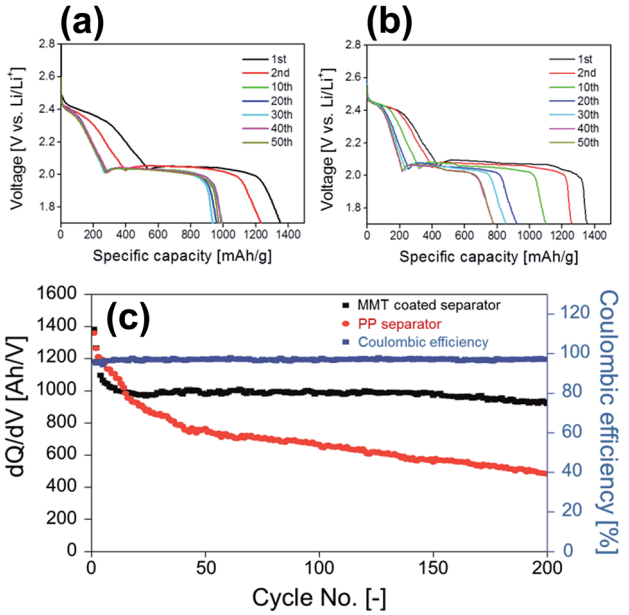

Fig. 10 Discharge curves of LiS cells using the MMT-coated separator (a) and as-received separator (b); comparison of cycle performance using the as-received separator and MMT-coated separator (c).

the anode. Fig. 10 displays the discharge profiles (Fig. 10(a) and (b)) and cyclability (Fig. 10(c)) determined from the lithium sulfur cells containing the MMT-coated separator and as-received separator. The initial discharge capacity was approximately 1380 mA h g^{-1} for both cells. However, only after 10 cycles, the capacity is significantly diminished for the cell using the as-received separator. The discharge capacities obtained from the as-received or MMT-coated separator after 200 cycles are 476 mA h g^{-1} and 924 mA h g^{-1} respectively. During the initial cycles, the decrease rate for the as-received separator cell is relatively small. However, after 5 cycles, the test cell with the MMT coated separator maintains the capacity of about 1000 mA h g^{-1}. The Coulombic efficiency of the cell using the MMT-coated separator shows *ca.* 97% after 200 cycles. The discharge profiles of all cells show commonly observed two plateaus, at approximately 2.4 and 2.1 V_{Li/Li^+}. These two plateaus indicate lithium polysulfide formation while the discharge process is advanced. It is accepted[29] that the first plateau represents the transformation of elemental sulfur to lithium polysulfide. From this result, it is clearly shown that the MMT-coated separator enhances the electrochemical performance of the cell. The MMT-coating layer enhances the cyclability by suppressing the diffusion of lithium polysulfide to the anode side. These results are in agreement with the Raman study.

Conclusion

In summary, a montmorillonite (MMT) coated separator was successfully manufactured using the phase inversion method for lithium sulfur batteries. As a cathode material, a sulfur–MWCNT composite was prepared through a simple method, consisting of 75 wt% sulfur and 25 wt% MWCNTs. The SEM

results confirmed that the MMT was homogeneously coated on the bare PP separator and that the sulfur was well dispersed on the surface of the MWCNTs. From the Raman study and zeta potential analysis, it is confirmed that the MMT layer coated on a bare PP separator can suppress the diffusion of dissolved sulfur to the anode side by repulsive electrostatic force between polysulfide and MMT. The electrochemical analysis showed that the MMT-coated separator makes it possible to maintain the discharge capacity of 924 mA h g^{-1} at 200 cycles from the initial capacity of 1380 mA h g^{-1}. Therefore, the MMT coating on a bare separator is a promising protective layer to improve the electrochemical capacity and cyclability by suppressing the diffusion of lithium polysulfide to the anode side in Li–S batteries.

Acknowledgements

This work was conducted under the framework of Research and Development Program of the Korea Institute of Energy Research (KIER) (B5-2414).

Notes and references

1 P. Gibot, M. Casas-Cabanas, L. Laffont, S. Levasseur, P. Carlach, S. Hamelet, J.-M. Tarascon and C. Masquelier, *Nat. Mater.*, 2008, **7**, 741–747.
2 B. Zhang, G. Chen, Y. Liang and P. Xu, *Solid State Ionics*, 2009, **180**, 398–404.
3 J.-H. Cho, J.-H. Park, M.-H. Lee, H.-K. Song and S.-Y. Lee, *Energy Environ. Sci.*, 2012, **5**, 7124–7131.
4 T. Ohzuku and R. J. Brodd, *J. Power Sources*, 2007, **174**, 449–456.
5 D. Marmorstein, T. Yu, K. Striebel, F. McLarnon, J. Hou and E. Cairns, *J. Power Sources*, 2000, **89**, 219–226.
6 N. Jayaprakash, J. Shen, S. S. Moganty, A. Corona and L. A. Archer, *Angew. Chem.*, 2011, **123**, 6026–6030.
7 X. Ji, K. T. Lee and L. F. Nazar, *Nat. Mater.*, 2009, **8**, 500–506.
8 H. Wang, Y. Yang, Y. Liang, J. T. Robinson, Y. Li, A. Jackson, Y. Cui and H. Dai, *Nano Lett.*, 2011, **11**, 2644–2647.
9 H. Yamin, A. Gorenshtein, J. Penciner, Y. Sternberg and E. Peled, *J. Electrochem. Soc.*, 1988, **135**, 1045–1048.
10 J. Shim, K. A. Striebel and E. J. Cairns, *J. Electrochem. Soc.*, 2002, **149**, A1321–A1325.
11 J. Wang, J. Yang, J. Xie, N. Xu and Y. Li, *Electrochem. Commun.*, 2002, **4**, 499–502.
12 C. Liang, N. J. Dudney and J. Y. Howe, *Chem. Mater.*, 2009, **21**, 4724–4730.
13 J. Wang, S. Chew, Z. Zhao, S. Ashraf, D. Wexler, J. Chen, S. Ng, S. Chou and H. Liu, *Carbon*, 2008, **46**, 229–235.
14 J. Guo, Y. Xu and C. Wang, *Nano Lett.*, 2011, **11**, 4288–4294.
15 R. G. Chaudhuri and S. Paria, *J. Colloid Interface Sci.*, 2010, **343**, 439–446.
16 W. Ahn, K.-B. Kim, K.-N. Jung, K.-H. Shin and C.-S. Jin, *J. Power Sources*, 2012, **202**, 394–399.
17 G. G. Kumar, K. S. Nahm and R. N. Elizabeth, *J. Membr. Sci.*, 2008, **325**, 117–124.
18 M. Wang, F. Zhao, Z. Guo and S. Dong, *Electrochim. Acta*, 2004, **49**, 3595–3602.
19 M. J. Koh, H. Y. Hwang, D. J. Kim, H. J. Kim, Y. T. Hong and S. Y. Nam, *J. Mater. Sci. Technol.*, 2010, **26**, 633–638.
20 M. Raja, T. P. Kumar, G. Sanjeev, L. Zolin, C. Gerbaldi and A. M. Stephan, *Ionics*, 2014, **20**, 943–948.
21 J. Nunes-Pereira, A. C. Lopes, C. M. Costa, R. Leones, M. M. Silva and S. Lanceros-Mendez, *Electroanalysis*, 2012, **24**(11), 2147–2156.
22 J. H. Chang and Y. U. An, *J. Polym. Sci., Part B: Polym. Phys.*, 2002, **40**, 670–677.
23 Y.-P. Wang, X.-H. Gao, R.-M. Wang, H.-G. Liu, C. Yang and Y.-B. Xiong, *React. Funct. Polym.*, 2008, **68**, 1170–1177.
24 Z. W. Seh, W. Li, J. J. Cha, G. Zheng, Y. Yang, M. T. McDowell, P.-C. Hsu and Y. Cui, *Nat. Commun.*, 2013, **4**, 1331.
25 Y. Yang, G. Yu, J. J. Cha, H. Wu, M. Vosgueritchian, Y. Yao, Z. Bao and Y. Cui, *ACS Nano*, 2011, **5**, 9187–9193.
26 G. Zheng, Y. Yang, J. J. Cha, S. S. Hong and Y. Cui, *Nano Lett.*, 2011, **11**, 4462–4467.
27 S. Dörfler, M. Hagen, H. Althues, J. Tübke, S. Kaskel and M. J. Hoffmann, *Chem. Commun.*, 2012, **48**, 4097–4099.
28 J.-T. Yeon, J.-Y. Jang, J.-G. Han, J. Cho, K. T. Lee and N.-S. Choi, *J. Electrochem. Soc.*, 2012, **159**, A1308–A1314.
29 P. G. Bruce, S. A. Freunberger, L. J. Hardwick and J.-M. Tarascon, *Nat. Mater.*, 2012, **11**, 19–29.